Rotating-polarization CARS microscopy: combining chemical and molecular orientation sensitivity

Giuseppe de Vito,[1,2,*] Angelo Bifone,[1] and Vincenzo Piazza[1]

[1]*Center for Nanotechnology Innovation @NEST, Istituto Italiano di Tecnologia, Piazza San Silvestro 12, I-56127 Pisa, Italy*

[2]*NEST, Scuola Normale Superiore, Piazza San Silvestro 12, I-56127 Pisa, Italy*

[*]*giuseppe.devito@sns.it*

Abstract: Coherent Anti-Stokes Raman Spectroscopy (CARS) is a non-linear process in which the energy difference of a pair of incoming photons matches the energy of the vibrational mode of a molecular bond of interest. This phonon population is coherently probed by a third photon and anti-Stokes radiation is emitted. Here a novel approach to CARS microscopy is presented yielding the intensity of the anti-Stokes emission, the directionality the molecular bonds of interest, and their average orientation. Myelinated axons in fixed mouse-brain slices have been imaged by RP-CARS. We were able to detect the local average direction of the acylic chains of membrane phospholipids and their spatial anisotropy. This novel method may impact the study of healthy brain circuitry as well as demyelinating diseases or other pathological states associated with altered neural connectivity.

OCIS codes: (300.6230) Spectroscopy, coherent anti-Stokes Raman scattering; (180.4315) Nonlinear microscopy; (180.5655) Raman microscopy; (180.6900) Three-dimensional microscopy; (190.4380) Nonlinear optics, four-wave mixing.

References and links

1. P. Maker and R. Terhune, "Study of optical effects due to an induced polarization third order in the electric field strength," Phys. Rev. **137**(3A), A801–A818 (1965).
2. J. X. Cheng and X. S. Xie, "Coherent anti-Stokes Raman scattering microscopy: instrumentation, theory, and applications," J. Phys. Chem. B **108**(3), 827–840 (2004).
3. C. L. Evans, E. O. Potma, M. Puoris'haag, D. Côté, C. P. Lin, and X. S. Xie, "Chemical imaging of tissue in vivo with video-rate coherent anti-Stokes Raman scattering microscopy," Proc. Natl. Acad. Sci. U.S.A. **102**(46), 16807–16812 (2005).
4. C. L. Evans and X. S. Xie, "Coherent anti-Stokes Raman scattering microscopy: chemical imaging for biology and medicine," Annu Rev Anal Chem (Palo Alto Calif) **1**(1), 883–909 (2008).
5. J. X. Cheng, S. Pautot, D. A. Weitz, and X. S. Xie, "Ordering of water molecules between phospholipid bilayers visualized by coherent anti-Stokes Raman scattering microscopy," Proc. Natl. Acad. Sci. U.S.A. **100**(17), 9826–9830 (2003).
6. A. V. Kachynski, A. N. Kuzmin, P. N. Prasad, and I. I. Smalyukh, "Coherent anti-Stokes Raman scattering polarized microscopy of three-dimensional director structures in liquid crystals," Appl. Phys. Lett. **91**(15), 151905 (2007).
7. F. Munhoz, H. Rigneault, and S. Brasselet, "Polarization-resolved four-wave mixing microscopy for structural imaging in thick tissues," J. Opt. Soc. Am. B **29**(6), 1541–1550 (2012).
8. J. X. Cheng, L. D. Book, and X. S. Xie, "Polarization coherent anti-Stokes Raman scattering microscopy," Opt. Lett. **26**(17), 1341–1343 (2001).
9. A. Volkmer, L. D. Book, and X. S. Xie, "Time-resolved coherent anti-Stokes Raman scattering microscopy: Imaging based on Raman free induction decay," Appl. Phys. Lett. **80**(9), 1505–1507 (2002).
10. Y. Fu, T. B. Huff, H.-W. Wang, J.-X. Cheng, and H. Wang, "Ex vivo and in vivo imaging of myelin fibers in mouse brain by coherent anti-Stokes Raman scattering microscopy," Opt. Express **16**(24), 19396–19409 (2008).
11. E. Bélanger, S. Bégin, S. Laffray, Y. De Koninck, R. Vallée, and D. Côté, "Quantitative myelin imaging with coherent anti-Stokes Raman scattering microscopy: alleviating the excitation polarization dependence with circularly polarized laser beams," Opt. Express **17**(21), 18419–18432 (2009).

#178788 - $15.00 USD Received 26 Oct 2012; revised 30 Nov 2012; accepted 30 Nov 2012; published 18 Dec 2012

12. H. Wang, Y. Fu, P. Zickmund, R. Shi, and J. X. Cheng, "Coherent anti-Stokes Raman scattering imaging of axonal myelin in live spinal tissues," Biophys. J. **89**(1), 581–591 (2005).
13. C. Shang and H. Hsu, "The spatial symmetric forms of third-order nonlinear susceptibility," IEEE J. Quantum Electron. **23**(2), 177–179 (1987).
14. R. W. Hellwarth, "Third-order optical susceptibilities of liquids and solids," Prog. Quantum Electron. **5**, 1–68 (1979).
15. M. Axer, K. Amunts, D. Grässel, C. Palm, J. Dammers, H. Axer, U. Pietrzyk, and K. Zilles, "A novel approach to the human connectome: ultra-high resolution mapping of fiber tracts in the brain," Neuroimage **54**(2), 1091–1101 (2011).
16. M. D. Budde and J. A. Frank, "Examining brain microstructure using structure tensor analysis of histological sections," Neuroimage **63**(1), 1–10 (2012).

1. Introduction

Optical microscopy has steadily evolved in the last few decades from a tool aimed at increasing the resolving power and magnification of the human eye to a powerful analytical technique. The introduction of confocal fluorescence microscopy, together with the development of a broad range of specific fluorophores, has enabled high-resolution imaging with chemical contrast, biological selectivity, and microenvironmental sensitivity. However, such flexibility comes at a cost: fluorophores often modify the biological and chemical properties of the target molecule and can perturb the cell as a whole. Moreover, photobleaching and phototoxicity are frequently an important issue.

CARS (Coherent anti-Stokes Raman Scattering) microscopy, a powerful and innovative technique based on the resonant and coherent generation of strong Raman anti-Stokes radiation by the target molecules [1], permits imaging of biological structures with excellent chemical selectivity and without the need of fluorescent probes.. The CARS signal conveys rich spectral information like traditional Raman microimaging, but the coherent build-up of the light field and the use of pulsed lasers yield intensities that are typically several orders of magnitude stronger than spontaneous Raman, thus enabling imaging at high frame rates and low laser power levels [2–4].

However, a quantitative interpretation of CARS, or – more generally – of four-wave mixing spectroscopy, images is complicated by the presence of the non-resonant background (NRB) and by polarization-dependent selection rules [5–7] that may introduce artifacts in the measured intensities. Several methods were proposed in the literature to reduce NRB [8, 9] and polarization-dependent effects [10, 11].

Here we show that it is possible to take advantage [11] of the polarization-dependent selection rules to detect the local microscopic orientation of the chemical bonds under investigation. To this end, we propose a CARS microscope based on a rotating polarization plane of the pump and probe beams. By means of RP-CARS it is possible to visualize the degree – within the optical point spread function (PSF) – of orientation anisotropy of selected molecular bonds and to detect their average orientation direction.

Brain white matter gives a strong CARS signal from the CH_2 bonds around 2850 cm^{-1} due to the lipid-rich myelin [12]. Myelin is a highly-ordered structure, in which many lipid-enriched, densely compacted phospholipid bilayers are spirally rolled up around the cylindrical axons. The linear acyl chains of the phospholipid molecules present a perpendicular orientation with respect to the myelin surface. Therefore, in a myelinated nerve fiber, a large number of molecular bonds are ordered around a radial axis of symmetry. Such a strong molecular anisotropy and symmetry make RP-CARS an ideal tool to investigate cerebral white matter.

2. Experimental techniques and materials

2.1 The RP-CARS microscope

The RP-CARS setup is based on a custom-built broadband implementation and is schematically shown in Fig. 1. 800-nm pump and probe beams are generated by a Ti-Sa

#178788 - $15.00 USD Received 26 Oct 2012; revised 30 Nov 2012; accepted 30 Nov 2012; published 18 Dec 2012

pulsed laser and spectrally narrowed by a pair of bandpass filters (labeled as 3-nm BP in Fig. 1) with a full width at half maximum (FWHM) of 3 nm. Approximately 750-fs pulses are sent to a rotating half-wave retarder (R-λ/2) through a telescopic beam expander. A broadband Stokes radiation (covering a wavelength range from 450 nm to 1200 nm) is generated by a non-linear crystal (SCG) pumped by a fraction of the 800-nm pulses diverted from the pump beam by means of a beam splitter (BS). In order to excite the symmetric stretch vibration of the CH_2 bonds, a spectral region ranging from 1000 nm to 1100 nm is selected from the broadband radiation by means of a combination of short-wave and long-wave pass filters (not shown in the figure). An achromatic quarter-wavelength retarder (λ/4) is employed to transform the linearly polarized Stokes pulses into circularly polarized radiation. With respect to the approach described in Ref [10], where all the polarizations of the pump, Stokes, and probe beam were kept linear and parallel to each other at the sample, our implementation consists of a circularly-polarized Stokes beam and a (rotating) linearly-polarized pump and Stokes beam. This choice avoids a few drawbacks of the all-linear-polarization approach: i) rotating the Stokes and pump-and-probe beams with the same half-wave retarder leads to small ellipticity of at least one of the beams due to their different wavelengths, even with an achromatic retarder; ii) rotating the Stokes and pump-and-probe beams with two different half-wave retarders would be technically challenging because the retarders would need to be rotated exactly at the same frequency and phase. On the contrary, in our approach the rotating half-wave retarder can be matched to the frequency of the narrowband pump-and-probe beam and the Stokes-beam-polarization circularity can be obtained and tested at the sample by carefully adjusting a quarter-wavelength retarder.

A second quarter-wavelength retarder is introduced in the pump and probe path in order to compensate for polarization distortions caused by the 818-nm long-pass dichroic filter (D). The latter recombines the pump and probe pulses with the Stokes ones. Temporal overlap between the pulses is achieved by adjusting a delay line (DL) on the Stokes-pulse path. The pulses are then routed to the high-numerical-aperture lens (Obj) through a pair of galvo-scanning mirrors (XY), a scan lens and a tube lens. The CARS signal is collected from the sample (S) by a condenser lens (Cond), filtered with a band-pass filter (BP) centered at 650 nm with a FWHM of 10 nm, and routed to a red-sensitive photomultiplier tube (PMT).

The output of the PMT is fed into a lock-in amplifier, whose reference frequency is derived by a Hall-effect sensor (HS) mounted in proximity to the electric brushless motor that drives the R-λ/2. The HS outputs two TTL pulses for each complete rotation of the retarder and therefore this TTL signal has the same frequency of the time-dependent pump-and-probe polarization and a fixed phase delay with respect to it. For conventional CARS imaging, the PMT output is also sent to a data acquisition/generation board that also controls the two galvo mirrors.

#178788 - $15.00 USD Received 26 Oct 2012; revised 30 Nov 2012; accepted 30 Nov 2012; published 18 Dec 2012

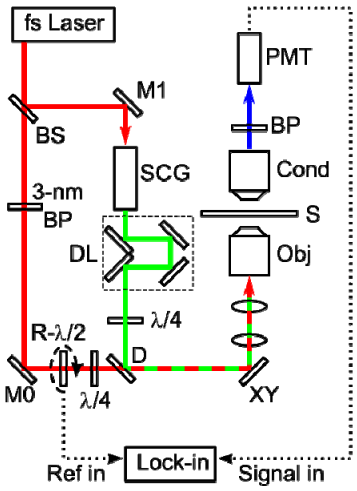

Fig. 1. Schematic representation of the RP-CARS setup. The 800-nm pulses from the laser (fs Laser), shown as red lines, are split by a beam splitter (BS) and routed to the supercontinuum generator (SCG) and, through two 3-nm bandpass filters (3-nm BP) centered at 800 nm, to the rotating λ/2 retarder (R-λ/2). The linearly-polarized broadband radiation (green lines) is delayed by a delay line (DL), transformed into circularly polarized light by a λ/4 retarder (λ/4), and recombined with the 800-nm radiation by means of a dichroic mirror (D). A second λ/4 retarder in the pump and probe path allows compensating for polarization distortions caused by D. The two are then routed to the high-numerical-aperture lens (Obj) through a pair of galvo-scanning mirrors, a scan lens and a tube lens. CARS signal is collected from the sample (S) by a condenser lens (Cond), band-pass filtered (BP), and routed to a photomultiplier tube (PMT). M0 to M2 are silver-coated mirrors. The output of the PMT is measured by phase-sensitive techniques by means of a lock-in amplifier. The reference phase and frequency for the lock-in amplifier is generated by a Hall sensor in close proximity to the rotor of the brushless motor that rotates R-λ/2.

2.2 Biological samples preparation

Adult wild type mice were perfused with 4% paraformaldehyde. The fixed brains were extracted from the skull and cut with a vibratome in coronal slices of 100 μm or 150 μm thickness. Slices were then mounted on standard microscopy slides in the presence of Phosphate Buffer Saline (PBS) solution and finally sealed with a glass cover slip and nail polish.

3. Theory

Following Refs [10, 13], the third-order susceptibility of the linear acyl chains of the phospholipidic membranes of the myelin layers can be described by a fourth-rank tensor containing just four independent coefficients: c_{11}, c_{16}, c_{18}, c_{33}. Given linearly polarized pump-and-probe beams, with a polarization plane rotating at an angular velocity ω, and a circularly-polarized Stokes beam, the time-dependent CARS-signal intensity is proportional to:

$$I_{CARS}(t) = I_p^2 I_S [A_{dc} + A_{2\omega} e^{(2i\omega t + i\varphi)} + A_{4\omega} e^{(4i\omega t + i\varphi)}],$$

where I_p and I_S are the intensities of the pump-and-probe beams and of the Stokes beam respectively, and:

#178788 - $15.00 USD Received 26 Oct 2012; revised 30 Nov 2012; accepted 30 Nov 2012; published 18 Dec 2012

$$A_{dc} = 3c_{11}^2 + 2c_{11}c_{16} + 14c_{16}^2 + 2c_{33}c_{16} + 3c_{33}^2$$
$$A_{2\omega} = 4\left(c_{11}^2 - c_{33}^2\right) \quad (1)$$
$$A_{4w} = c_{11}^2 - 2c_{11}c_{16} - 6c_{16}^2 - 2c_{33}c_{16} + c_{33}^2.$$

Here φ is the angle at $t = 0$ between the polarization plane and the acyl chains. By employing phase-sensitive techniques, the three terms A_{dc}, $A_{2\omega}$, $A_{4\omega}$, and the phase φ, that represents the local orientation of the dipoles, can be readily measured.

In order to get accurate results, it is of paramount importance to compensate for polarization distortions, due to different retardations of the vertical and horizontal components of the polarizations introduced by the dichroic mirror (D). To this end, the CARS signal coming from the glass cover slip can be exploited as a reference, since it contains exclusively an isotropic, non-resonant contribution, which can be described by the following third-order susceptibility [14]:

$$\chi_{ijkl} \propto \delta_{ij}\delta_{kl} + \delta_{ik}\delta_{jl} + \delta_{il}\delta_{jk}.$$

In the ideal case of a circularly polarized Stokes beam and rotating perfectly-linear pump-and-probe beams, it is easy to see that $I_{CARS}(t)$ is a constant. On the contrary, if the Stokes beam is elliptical rather than perfectly circular, the CARS signal contains also a second-harmonic component:

$$I_{CARS}(t) = I_p^2 I_S \left[B_{dc} + B_{2\omega} e^{(2i\omega t + i\varphi)} \right],$$

where B_{dc} and $B_{2\omega}$ depend on the amount of distortion from a perfectly circularly polarized beam and φ depends on the orientation of the ellipse axis.

The other possible deviation from the ideal case stems from a retardation imposed by D on the horizontal or vertical components of the polarization of the pump-and-probe beams. In this case $I_{CARS}(t)$ contains both second-harmonic and fourth-harmonic contributions in addition to a constant term.

These considerations suggest that it is possible to minimize polarization distortion effects by focusing the microscope into a glass slide and tune the orientation of the two quarter-wavelength retarders in order to minimize the second- and fourth-harmonic component of the signal. Ratios between the ac component of the signal at 2ω and the dc signal smaller than 0.5% could routinely be achieved.

4. Results and discussion

The mouse brain is a complex animal tissue, where gray matter (cell somata and non-myelinated axons) is interposed with white matter (myelinated and non-myelinated axons). White matter gives a strong CARS signal from the highly ordered CH_2 bonds at 2850 cm^{-1} due to the lipid-rich myelin.

The incident laser light is linearly polarized in traditional CARS microscopes. This usually leads to artifacts similar to the one depicted in Fig. 2 that shows an individual myelinated axon placed perpendicularly to the imaging plane: chemical bonds aligned with the polarization plane of the incident light generate a stronger CARS signal with respect to those aligned perpendicularly. Such artifacts can be mitigated by post processing two images acquired with orthogonal polarizations [10] or by using circularly polarized light [11].

#178788 - $15.00 USD Received 26 Oct 2012; revised 30 Nov 2012; accepted 30 Nov 2012; published 18 Dec 2012

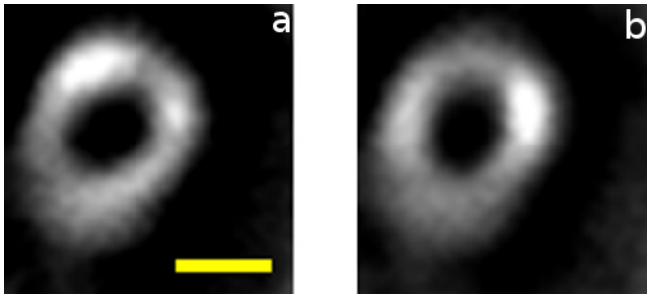

Fig. 2. Polarization-dependent artifact in a CARS image of a single nerve axon in transverse section (CH and CH_2 bonds). (a) The polarization-dependent artifact is evident when linearly-polarized light is used. In this case the CH and CH_2 chemical bonds aligned with the polarization plane of the incident light (vertical in the image) generate a stronger CARS signal. (b) Same as a) but using a perpendicular polarization plane of the incident light (horizontal in the image). The pump and probe beam and the Stokes beam power was respectively 30 mW and 12 mW. Scale bar: 0.5 μm.

RP-CARS exploits, rather than mitigate, polarization selection rules in order to gather information on the local orientation anisotropy of chemical bonds. The radius signal originated by the lock-in amplifier ($A_{2\omega}$, when the second harmonic with respect to the reference frequency is selected) is a measure of the local – within the PSF volume – anisotropy of the molecular-bond orientation. Also, using RP-CARS it is possible to generate images free from such artifacts by exploting the A_{dc} signal, as shown in Fig. 3(a). The phase of the signal, detected by the lock-in, corresponds to the average orientation of such bonds. In order to visualize both signals at the same time, we used the HSB color space, where the $A_{2\omega}$ signal is mapped onto the brightness channel and the phase signal onto the hue. Saturation is kept at the maximum value. This picturing method is described in Fig. 3, showing the same single nerve axon displayed in Fig. 2.

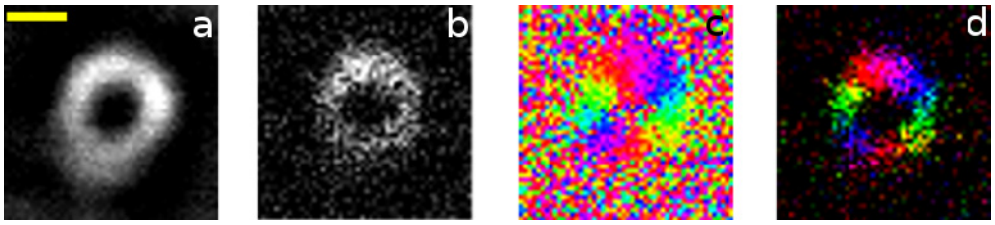

Fig. 3. RP-CARS imaging of the same single nerve axon as in Fig. 2 (CH_2 bonds, transverse section). (a) Image constructed using A_{dc}. Compared to the images in Fig. 2 it is free from the polarization artifacts. (b) Image constructed using $A_{2\omega}$ (bright pixels indicate that the signal value varies strongly as a function of the light polarization orientation). (c) Image of the phase of the signal collected from the same region (the colors indicate different light-polarization orientations). (d) RP-image constructed using the image in b) as brightness value and the one in c) as hue value. The myelin sheaths change color smoothly, covering all the possible orientations. The power levels were the same as in Fig. 2. The scale bar length is 0.5 μm.

The $A_{2\omega}$ signal and the phase signal from the lock-in are shown in Fig. 3(b) and Fig. 3(c) respectively. The final image obtained according to the approach described above is displayed in Fig. 3(d). The phase signal acquires random values when the signal-to-noise ratio is very small, but this artifact does not affect the final fusion image because the brightness is small too.

The wall of the axon changes color smoothly, covering all the possible orientations, owing to the directionality of the CH_2 bonds in the phospholipid bilayer that forms the myelin: the

#178788 - $15.00 USD Received 26 Oct 2012; revised 30 Nov 2012; accepted 30 Nov 2012; published 18 Dec 2012

CH_2 bonds of the phospholipid acylic chains always lay in planes parallel to the surface of the membrane, therefore in the circumference of the axons wall they gradually assume all the possible orientations. As noted above, using lock-in techniques gives access to A_{dc}, $A_{2\omega}$, and $A_{4\omega}$ and, in turns, to the coefficients of the third-order susceptibility (up to a proportionality factor). Focusing our microscope on a myelinated fiber wall yielded A_{dc}=150 mV, $A_{2\omega}$=38.5 mV, and $A_{4\omega}$=2.5 mV. Inverting Eq. (1) the following values for the coefficients can be calculated: c_{11} = 1, c_{16} = 0.28, c_{33} = 0.75 (c_{18} is not accessible with in-plane only polarizations), in good agreement with values previously reported for fixed tissues [11].

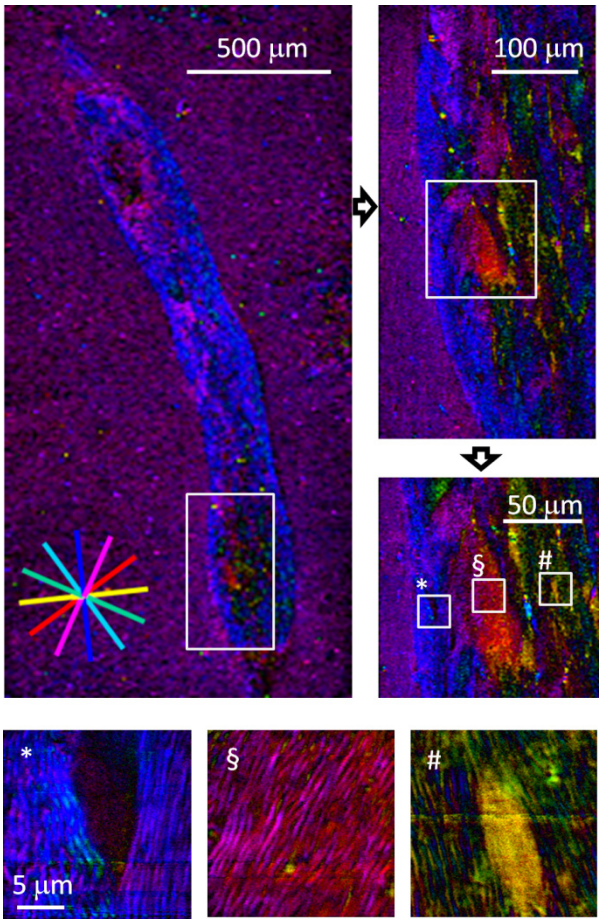

Fig. 4. Coronal section of the mouse brain anterior commissure imaged at different magnifications. This multi-scale acquisition shows the degree of local asymmetry in the direction of the acylic chains and their average spatial orientation (the color-coding scheme is described in the text). The white rectangles show the region magnified in the successive image of the series (indicated by an arrow). The colored lines in the top-left panel depict the color-to-orientation mapping. The last three images (*,§ and #) refer respectively to the three white rectangles in the preceding image. The pump and probe beam and the Stokes beam power was respectively 50 mW and 10 mW.

Figure 4 displays a series of images at increasing magnifications of a coronal section of mouse-brain anterior commissure. This multi-scale acquisition shows the degree of local asymmetry in the direction of the CH_2 bonds and its average spatial orientation (with the same color coding described above for Fig. 3) for very different spatial scales. Using the RP-CARS technique we were able to detect the presence and average direction of fiber bundles by

#178788 - $15.00 USD Received 26 Oct 2012; revised 30 Nov 2012; accepted 30 Nov 2012; published 18 Dec 2012

analyzing the intensity and color of that region (Fig. 4). A comparison between low magnification images (here low magnification means that the resolution is not enough to reveal the individual fibers) and high magnification images (resolution high enough to resolve the fibers) confirm that the presence of bright colors in the low-magnification images correlates to the presence of aligned fibers and that the color indicates the overall orientation of the fiber. With respect to existing techniques based on optical methods [15,16], our approach enables in addition chemical sensitivity, targeting selected molecular structures.

The laser power levels employed in our measurements (reported in the figure captions) were not found to produce any visible alteration of the tissues under analysis. Moreover, similar power levels have been reported in studies of live cells and shown not to cause any visible adverse effect [2].

RP-CARS images are also much less sensitive to contrast alterations caused by regions of different absorbance in complex thick biological samples. Figures 5(a) and 5(b) shows the CARS signal from two brain slices having different thicknesses, 100 μm and 150 μm respectively. Figure 5(a) reflects well the fact that the CH_2 signal from regions of abundant myelinated axons (white matter) is larger than that from grey matter. On the contrary Fig. 5(b) displays opposite contrast, owing to the fact that white matter scatters the signal more than grey matter and, above a threshold tissue thickness, the signal loss prevails. In Fig. 5(c), showing the same slice of Fig. 5(b), the $A_{2\omega}$ signal from the lock-in was normalized with respect to A_{dc}, recovering the expected contrast for the image.

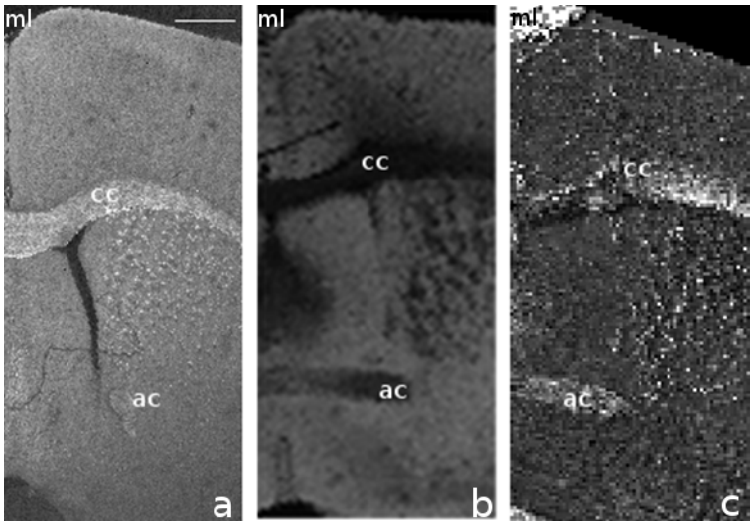

Fig. 5. A_{dc} and $A_{2\omega}$ signals of mouse brain slices (CH_2 bonds). (a) Conventional CARS image (linar polarizations) from a 100-μm-thick brain slice (bregma: 0.4 mm). (b) A_{dc} signal from a 150-μm-thick brain slice (bregma: –0.1 mm). Note that in (a) white matter (e.g., corpus callosum or anterior commissure) appears bright, whereas in (b) it appears dark. This effect is due to the different slice thickness: the thicker the slice, the more its dense white matter diffuses the CARS signal. (c) Image from the same brain slice shown in (b), but constructed using the $A_{2\omega}$ signal (divided by the A_{dc} signal): in this case the white matter appears bright as in (a). The medial longitudinal fissure, filled with aqueous solution, appears artifactually bright due to its low A_{dc} signal. cc: corpus callosum. ac: anterior commissure, its shape appears different in (a) with respect to (b) and (c) because of the diverse positioning of the coronal slice (distance to bregma). ml: medial longitudinal fissure. The pump and probe beam and the Stokes beam power was respectively 30 mW and 18 mW. Scale bar: 0.25 mm.

#178788 - $15.00 USD Received 26 Oct 2012; revised 30 Nov 2012; accepted 30 Nov 2012; published 18 Dec 2012

In the current implementation of RP-CARS, the image acquisition time is limited by the integration time of the lock-in amplifier, which has to sample a few rotation periods (T_R) of the polarization plane for each pixel in order to be able to perform the phase-detection algorithms. Since in our setup ω = 90 Hz, we employed integration times ranging from 20 ms to 50 ms. This limitation makes the image acquisition process rather slow: a 100x100-pixel image, in the most favorable case, is acquired in 200 s. Nevertheless, we envision that the acquisition time could be greatly reduced by performing the phase detection in a post-acquisition step by software processing. Indeed, it is possible to acquire an entire line of pixels of the image in a much shorter time than T_R. The same line could be sampled repeatedly, in such a way that the output of the PMT for each pixel (together with the output of the HS) is sampled many times during a rotation of the polarizer and for a few rotations. A post-processing step could then recover the phase and amplitude values for each pixel. With this approach an entire line could be imaged in 20-to-50 ms (i.e. the time now required for a single pixel) leading to a n-fold speedup for an $n \times n$ image.

4. Conclusions

We presented a novel microscopy technique derived from Coherent anti-Stokes Raman Scattering. We exploited the well known polarization-dependent artifacts characteristic of CARS to probe the average spatial orientation of the molecular bonds of interest by using a rotating half-wave plate to continuously change the polarization plane of the incident light and recovered orientation information via lock-in techniques.

Rotating Phase CARS is a very effective method to detect the orientation and the anisotropy of ordered molecular structures with radial symmetry, such as myelin.

We believe that this method may significantly impact the study of pathological states associated with altered neural connectivity and of the circuitry of the healthy brain. RP-CARS may also allow new insights in the investigation of the alteration in local myelin order in animal models of progressive demyelinating diseases such as multiple sclerosis.

Acknowledgments

We thank Dr. Alessandro Gozzi and Dr. Alberto Galbusera (Center for Nanotechnology Innovation @NEST, Istituto Italiano di Tecnologia) for providing mouse brain samples. We also acknowledge Dr. Massimo Pasqualetti and his staff (Università di Pisa) for assistance in brain slice preparation and Dr. Pasqualantonio Pingue (Scuola Normale Superiore) for careful reading of the manuscript.

#178788 - $15.00 USD Received 26 Oct 2012; revised 30 Nov 2012; accepted 30 Nov 2012; published 18 Dec 2012